LA-UR-18-23778 (Accepted Manuscript)

Effect of flow field geometry on operating current density, capacity and performance of vanadium redox flow battery

Maurya, Sandipkumar
Nguyen, Thanh Phong
Kim, Yu Seung
Kang, Qinjun
Mukundan, Rangachary

To be published in: Journal of Power Sources

DOI to publisher's version: 10.1016/j.jpowsour.2018.09.093

Permalink to record: http://permalink.lanl.gov/object/view?what=info:lanl-repo/lareport/LA-UR-18-23778

Effect of flow field geometry on operating current density, capacity and performance of vanadium redox flow battery

Sandip Maurya[a], Phong Thanh Nguyen[a], Yu Seung Kim[a], Qinjun Kang[b], Rangachary Mukundan[a,*]

[a]Materials Synthesis and Integrated Devices, MPA-11, Materials Physics and Applications Division, Los Alamos National Laboratory, Los Alamos, NM, 87544, USA

[b] Computational Earth Science, EES-16, Earth and Environmental Sciences Division, Los Alamos National Laboratory, Los Alamos, NM, 87544, USA

Highlights:

1. Conventional flow field shows low mass transport limitation and higher limiting current density at any flow rate.
2. Serpentine flow field offers better depth of discharge at low SOC.
3. Interdigitated outperforms serpentine and conventional flow fields at low current density and flow rates.
4. Electrode type is not the limiting factor in VRFB for higher power density applications.

Abstract:

Addition of flow fields in a vanadium redox flow battery (VRFB) tends to improve the peak power density when combined with carbon paper electrodes due to the uniform distribution of electrolyte throughout the electrodes. However, it is still unclear whether flow fields have a similar effect with graphite felt electrodes – a conventional thick electrode used in VRFBs. The VRFBs with felt electrodes reported in the literature show a large anomaly in the obtained power density. Therefore, in this work, we have evaluated three flow fields; namely serpentine, interdigitated and conventional type with felt electrodes and compared their performance with VRFBs using carbon paper electrodes under identical experimental conditions. The effects of flow rate was investigated on the cycling performance and polarization behavior of VRFBs with different flow fields. The capability of VRFBs for deep discharge was analyzed by obtaining polarization curves at different state of the charge. Electrolyte flow rate increases the maximum power density and limiting current densities for all flow fields because of better electrolyte distribution and less electrolyte residence time. Yet, flow fields show considerable mass transport limitation compared to conventional flow field. Even a VRFB assembled with serpentine flow field with carbon paper electrode exhibits lower maximum power density than conventional flow field using graphite felt electrodes. Computational fluid dynamic (CFD) modeling on flow fields for electrolyte transport and distribution confirms the experimental results.

1. Introduction

Renewable energy sources such as wind and solar are intermittent and need large-scale electrochemical energy storage (EES) alternatives [1]. The potential of vanadium redox flow batteries (VRFBs) as a grid-scale energy storage alternative is well documented [2-4]. The VRFB connected to the grid not only stores excess electricity but also helps with peak shaving, and grid-stabilization by providing energy during peak demand [5]. Moreover, thanks to its fast response to dynamic loads, VRFBs can also be used in hybrid distributed power generation systems along with fuel cells [6]. Intermittent energy production systems in combination with VRFBs can provide quite robust and sustainable power distribution. VRFBs possess distinct advantages over other flow battery chemistries for large-scale EES. VRFBs consist of positive electrolyte (VO^{2+}/VO_2^{+}) and negative electrolyte (V^{2+}/V^{3+}) dissolved in sulfuric acid or mixture of sulfuric acid – hydrochloric acid separated by an ion exchange membrane [7]. These redox couples in anolyte and catholyte are derived from vanadyl sulfate. Therefore, the cross-contamination, which is inevitable, does not result in the loss of electrolyte. Fortunately, spent and cross mixed electrolytes could be remixed and rebalanced for metal ion – acid concentration, which provides VRFBs a distinct edge over other flow battery technologies in terms of electrolyte costs [8].

The low energy density due to cross mixing and inherent solubility limit of vanadium sulfates in sulfuric acid, is a major hurdle for commercialization of VRFBs. Therefore, significant research has focused on the development of suitable membranes such as positively charged anion exchange, and porous membranes for minimal cross mixing [9-13]. While the use of mixed acid electrolyte has improved the solubility of vanadium species almost two fold, energy density of VRFB stands at <30 Wh L^{-1}, which is still considerably less than the capacity

of lithium-ion batteries which are >150 Wh L^{-1} [14]. Fortunately, increasing the volume of electrolytes can instantly increase the total capacity of VRFB while increasing the number of single cells in a stack increases the power output. Therefore, a simple operation of sizing up the electrolyte tank and cell stack can easily balance the effect of low energy density unlike other secondary batteries such as Li-ion battery where whole system needs to be built from scratch [15]. However, addition of each module consisting of membrane, electrodes, and bipolar plates further adds to the overall system costs. Therefore, improvement in the power density of VRFB can help improve efficiency and reduce the tank size and stack size for any given peak demand. The higher power density could be realized by high output current at operating voltage [16].

Several previous reports state that the power density of VRFBs are merely < 200 mW/cm^2 owing to the significant mass transport issues associated with the thicker graphite felt [17, 18]. Introduction of flow fields and the use of thin and dense carbon paper electrodes in combination with flow fields have greatly improved the power density (up to ~550 mW/cm^2) due to the better distribution of electrolyte and less parasitic pump loss [16, 19]. However, the improvement in power density was insignificant when felt used in conjunction with flow fields [17]. Davis *et al.* have recently shown that felt electrodes can compete with carbon paper electrodes in terms of VRFB performance under identical conditions [20]. Theoretically, polarization curves should not be notably different in the activation and ohmic region when matching concentration of electrolyte and membranes are utilized. The only notable difference could be observed in mass transport region due to use of the thick electrodes. However, five-fold increase seen with carbon paper indicates that the polarization curves of traditional VRFBs should be analyzed with more care. The polarization curves reported in the literature were analyzed under different operating conditions, cell size and electrolyte conditions, which

obscures their direct comparison. VRFBs are fundamentally transient systems like any other batteries, therefore, polarization curves should be obtained with quick scans of potential or current. Fast scans minimize the depletion of State of Charge (SOC) locally in the cell compartment while providing the proper polarization curves.

Therefore, in this study, we have investigated the VRFB with serpentine, interdigitated, conventional, and zero gap configuration with serpentine flow field for their polarization behavior and cycling performances. The improved method to record the polarization curves without depleting the SOC locally is used to compare the performances. The effects of flow fields, flow rate, SOC and cell geometries on polarization curves have been evaluated. We were able to achieve a power density of ~580 mW/cm^2 with optimized flow rate. Computational fluid dynamic (CFD) modeling of electrolyte diffusion and transport in the channels and electrodes are also used in this work to examine the effects of mass transport on the performance of flow field geometries and pressure drop. In this study, we are presenting comprehensive insights of VRFBs that can be further extended to any flow batteries.

2. Experimental

2.1 VRFB mass transport model

The computational domain consists of the bipolar plate with machined channels and the porous electrode graphite felt. The overall dimension of the flow cell area is 5 x 5 cm^2. Three types of flow field configuration were used in this study: conventional, interdigitated, and serpentine (as shown in Fig. 1). The dimensions of the serpentine channels are: groove width 0.7874 mm, groove depth 1.016 mm, 30 grooves; interdigitated channels are: groove width 0.7874 mm, groove depth 1.016 mm, manifold width 1.173 mm, manifold depth 2.54 mm. The

conventional flow field (CFF) does not have flow channels instead felt is placed in the 1.75 mm deep 5 x 5 cm^2 square trenches. The inlet flow rate was kept at 40 mL/min for simulation and compared to experiments. No slip boundary conditions applied at the 3 walls, and the outlet is a constant-pressure boundary conditions. Comsol Multiphysics version 5.3 was used in these simulations. The electrode is graphite felt with compressed thickness of 3.22 mm, porosity of 0.9, and permeability of 1 x 10^{-11} m^2 [21]. The flow distribution in the channel was solved using Navier-Stokes equation [22] as follows:

$$\nabla\cdot(\rho u) = 0 \quad (1)$$

$$\nabla\cdot(\rho u \otimes u - \mu\nabla u) = -\nabla(p + 2/3\mu\nabla\cdot u) + \nabla\cdot[\mu(\nabla u)T] \quad (2)$$

Flow distribution in the porous electrode was solved for using Darcy equation [22] :

$$u = -k\_p/\mu\nabla p \quad (3)$$

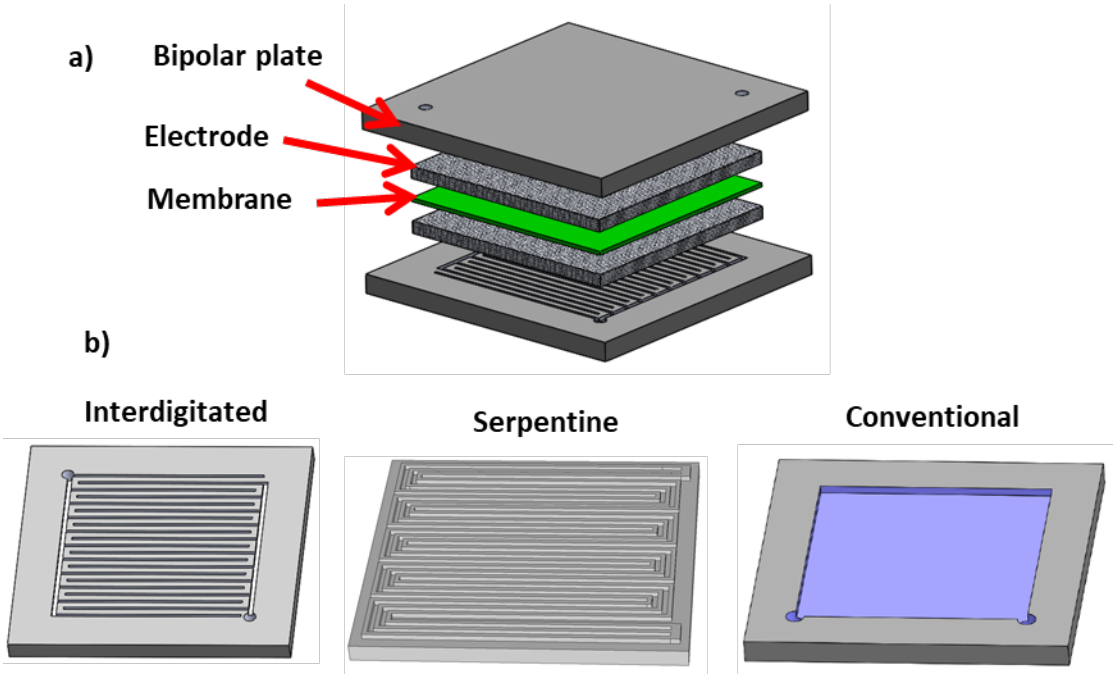

Figure 1. a) Flow battery assembly and b) flow patterns: interdigitated, serpentine and conventional.

2.2. VRFB single cell assembly

A VRFB single cell hardware was obtained from fuel cell technologies with 25 cm^2 active area. Fig. 1 shows the vital components of flow cell assembly used in this study. A single cell VRFB was comprised of; a Nafion membrane (Nafion® 212, 50.8 µm dry thickness, fuel cell store, USA), graphite felt electrodes (GFD 4.6EA, 4.6 mm thick, SGL technologies GmbH) or carbon paper (SGL 10 AA, 360 µm thick), bipolar plates with grooved flow fields (Pyrosealed, Poco® Graphite Inc, USA), gold plated current collectors and end plates.

Three flow patterns were tested: a three-channel serpentine (SFF), single channel interdigitated (IFF) and 1.75 mm deep conventional flow field (CFF) as shown in Fig. 1. Compression ratio was controlled to 30% by EPDM gaskets to avoid the change in permeability of felt electrode. Properties of graphite felt and carbon paper electrodes are presented in Table S1 (Supporting information). Carbon paper and graphite felts electrodes were thermally treated at 400 ^oC for 17 h prior to charge/discharge experiments. The Nafion® membrane was pretreated by immersion in 2.5 M sulfuric acid at room temperature for at least an hour and excess sulfuric acid was wiped from the surface before assembling in the single cell.

2.3. Electrolyte preparation

The electrolyte solution was prepared by dissolving 1.0 M vanadyl sulfate ($VOSO_4$ xH_2O, x =3 – 5, 97%, Sigma-Aldrich, USA) in 2.5 M sulfuric acid (H_2SO_4, Fisher Chemicals, USA). In order to wet the electrodes and remove trapped gases from the electrodes, both electrolyte reservoir were recirculated initially with 60 mL of electrolyte. Additional 60 mL of electrolyte solution was added to the positive electrolyte (catholyte) reservoir, twice the negative

electrolyte (anolyte) volume. Dry nitrogen gas was purged continuously through the anolyte reservoir to avoid the oxidation of V^{+2}. These electrolytes were charged under constant voltage at 1.8 V until catholyte converted to ~100% V^{+5} and anolyte ~100% V^{+2}. Then, 60 mL of catholyte was removed which left 60 mL of V^{+2} and V^{+5} in anolyte and catholyte reservoir, respectively. Flow rates of electrolyte was maintained at 40 mL/min throughout the experiments using Masterflex® peristaltic pump and acid resistant tygon® tubings (L/S 16).

2.4. VRFB single cell test

Polarization curves were measured by fuel cell station (fuel cell technologies) equipped with potentiostat and 40 A load box. High frequency resistance measured at 1000 Hz was used to get the iR-corrected polarization curves. Polarization curves were recorded by discharging the cell to 100, 75, 50 and 25% SOC for each flow field type. Furthermore, flow rate effects were also studied at 100% SOC. Each voltage step lasted 5 seconds for the polarization curve measurement. Since no significant increase in cell temperature was observed, no effort was made to control the temperature. The charge/discharge cycling tests were performed at 40, 80, 120, 160 and 200 mA/cm^2 and cutoff voltages fixed between 0.8 V and 1.8 V using a battery cycler (Scribner flow battery station).

3. Results and Discussion:

3.1 Simulation

The pressure and velocity distribution in the channels and electrodes of all three flow field configurations were obtained from the simulation. For IFF, the pressure drop across the cell is 600 Pa with higher pressures at the inlet manifold and channels connected to the inlet

manifold, and lower pressures at the outlet manifold and channels connected to this manifold (Fig. 2a). The velocity distribution in the channels is higher in the inlet manifold and lower at the end of the side channels (Fig. 2b). Velocity in the electrode is 3 orders of magnitude smaller than velocity in the channels due to porous media flow behavior (Fig. 2c). In the electrode, the velocity is highest at the ends of the side channels where the fluid in the channel is forced to flow under the channel into the electrode to pass to the next channel or outlet manifold.

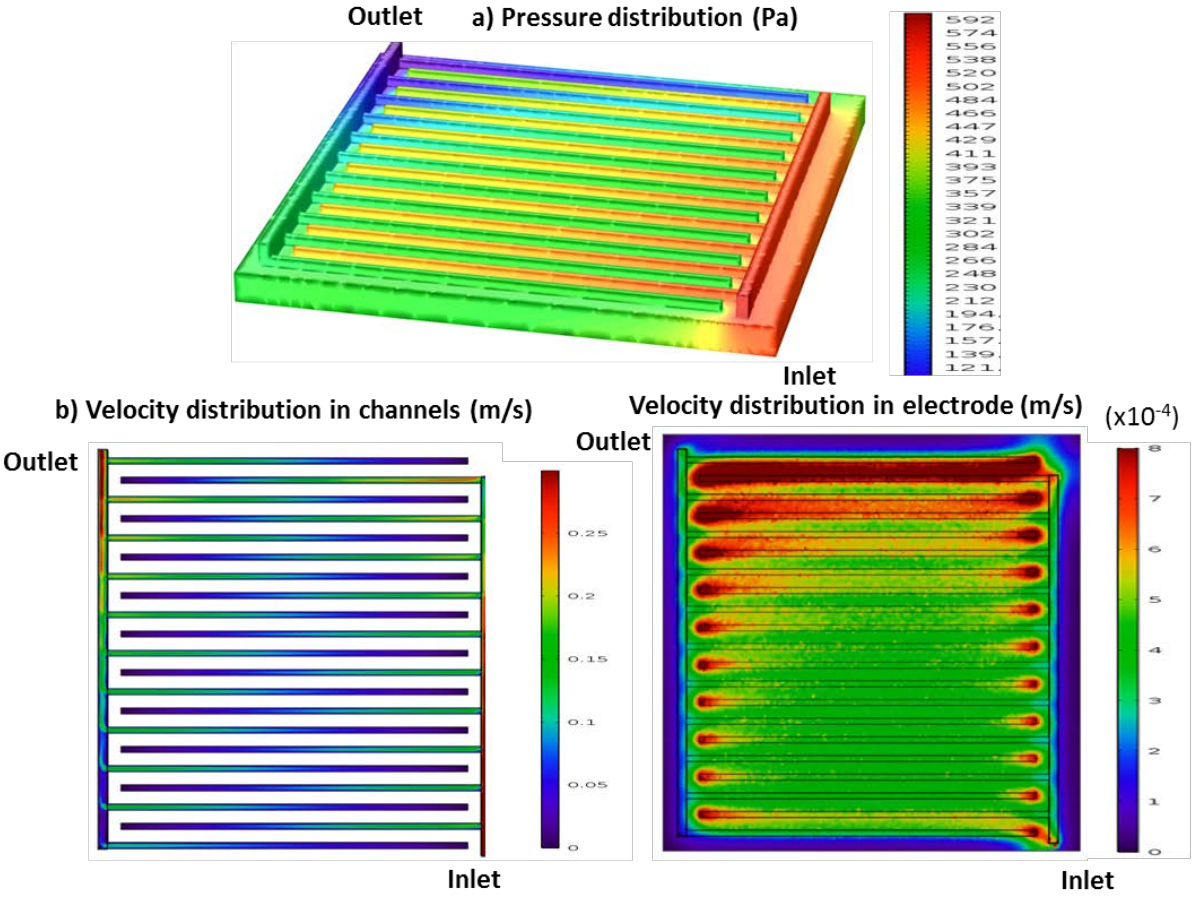

Figure 2. Pressure and velocity distribution with interdigitated flow field pattern a) pressure distribution in the channels and electrode b) velocity distribution in channels c) velocity distribution in the electrode.

For SFF, the pressure drop across the cell is 7000 Pa with the higher pressures in the inlet region and low pressures in the outlet region in both channel and electrode (Fig. 3a). The velocity in the channels is higher at the inlet and in the center of the channels which is characteristic of laminar flow in rectangular cross section channels (Fig. 3b). Velocity in the electrode is about 2 orders of magnitude smaller than velocity in the channels due to porous media flow behavior (Fig. 3c). In the electrode, the velocity is highest in the areas not directly underneath the gas channels due to pressure drops along the channels and fluid being forced to flow into the electrode to downstream channels.

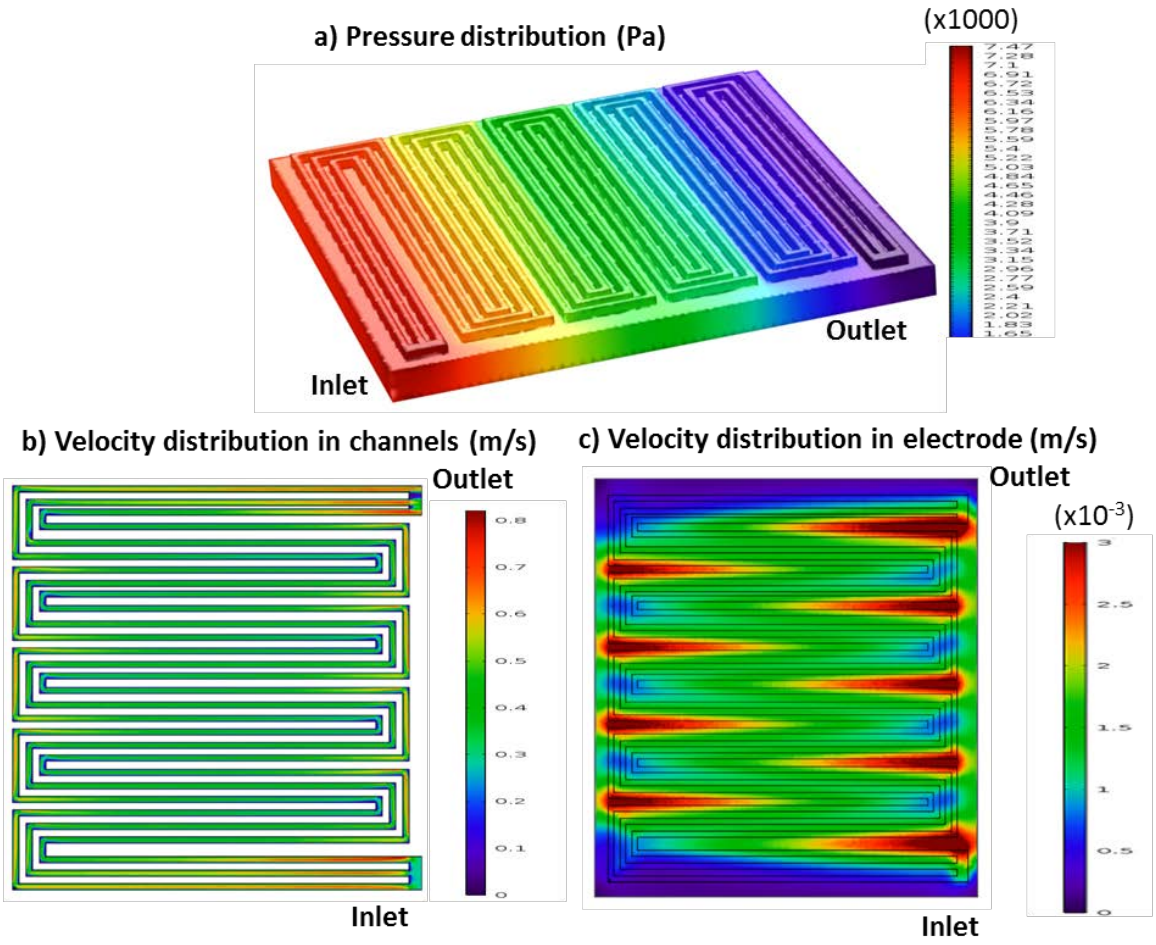

Figure 3. Pressure and velocity distribution with serpentine flow field pattern a) pressure distribution in the channels and electrode b) velocity distribution in channels c) velocity distribution in the electrode.

For CFF, the pressure drop across the cell is 65,000 Pa with higher pressures in the inlet region and lower pressures in the outlet region (Figure 4a). The velocity in the electrode is almost uniform with a magnitude of about $1x10^{-2}$ m/s (Figure 4b).

In comparing the three flow field patterns: the pressure drop in the flow through electrode in CFF is the highest with a value of ~ 65,000 Pa which is one order of magnitude higher than SFF and two orders of magnitude higher than IFF. These calculated pressure drop values also

match with the literature [23]. The pressure drop was also measured by flowing water and 3.5 M NaCl solution into the VRFB single cell for the sake of comparison. Interestingly, the measured pressure drop follows the similar trend with the values from simulations (Supporting information, Table S2). The flow through electrode in CFF also has the highest velocities in the electrode with a value of ~1x10^{-2} m/s which is one order of magnitude higher than SFF and two orders of magnitude higher than the IFF. Higher velocity results in better convective mass transport. These results directly support the experimental mass transport effects observed in the polarization curves measurements which also found that the flow through electrode design has the best cell performance. The experimental results are discussed in subsequent sections.

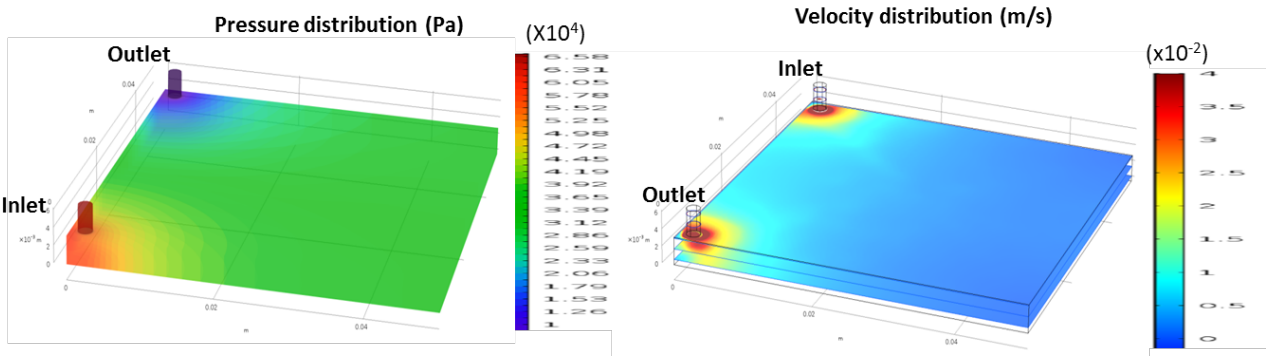

Figure 4. Pressure and velocity distribution with flow through electrode pattern in CFF a) pressure distribution in the channels and electrode b) velocity distribution in channels c) velocity distribution in the electrode.

3.2 Effect of flow fields on the cell performance at different current densities

In order to eliminate the effect of vanadium crossover and hence improve the accuracy of measurement, equivalent experimental conditions, concentration of electrolytes and membrane were used. The Coulombic, voltage and energy efficiencies of respective flow fields along with discharge capacity are illustrated in Fig. 5 (a, b, c and d) between current densities of 40 and 200

mA/cm^2. The CE ranges between 95 to 100% depending on the operating current density and type of flow field (Fig. 5(a)). The CEs increase with current density for all flow fields attributed to the shorter time required to achieve charge/discharge cut off voltages at higher currents. Shorter charge/discharge time results in lower crossover of vanadium species during charge/discharge cycle. In general, ohmic losses and over-potential tend to increase with increasing current density. Consequently, The VE drops dramatically from > 90% at 40 mA/cm^2 to 52% at 200 mA/cm^2 for IFFs. Similar but less dramatic trend is also seen for SFF and CFF as shown in Fig 5(b). The lower VE and ~100% CE for IFF indicate that the single cell with IFF has reached the voltage cut-off limit before complete charge or discharge due to the mass transport losses associated with lower electrolyte velocity in the electrodes.

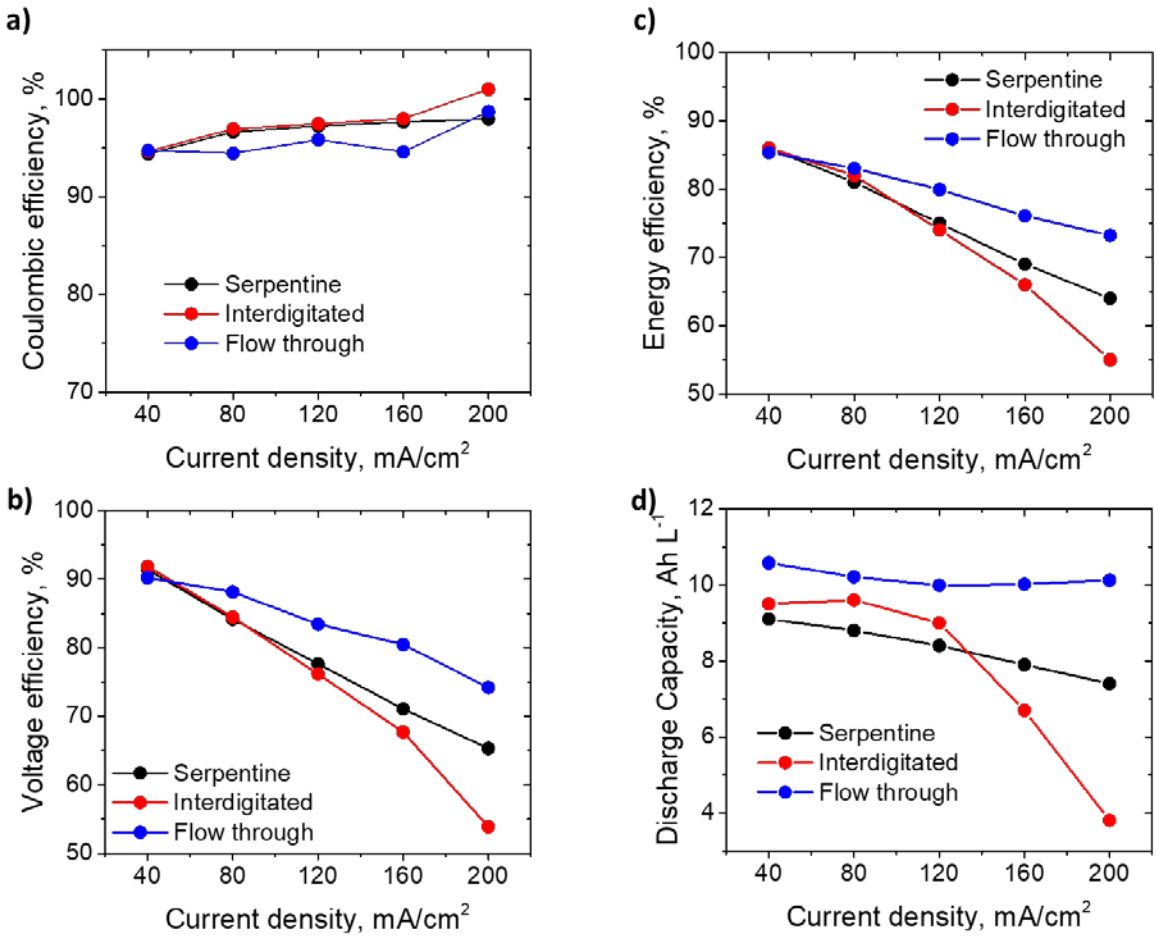

Figure 5. VRFB single cell performance with respect to flow field geometries; (a) Coulombic efficiencies; (b) Voltage efficiencies; (c) Energy efficiencies; (d) discharge capacities (all the efficiencies and capacities are average of 20 cycles, temperature: 25 ^{o}C, flow rate: 40 mL/min)

The EE of ~85% of achieved with all flow field geometries at 40 mA/cm^2 (as shown in Fig 5(c)). However, with increasing current density EE tanks up to 55% for IFF. The single cell with CFF showed minimum decline in EE with increasing current density and settled at 75% at 200 mA/cm^2. On the other hand, under equivalent condition SFF could achieve only 65% EE. As expected from the simulations, CFF has shown the higher EEs at high current density operations. This could be attributed to the better mass transport at higher current densities due to the larger velocities within the electrode. Although, typical charge/discharge cycling tests determine the

CE, VE and EE; they do not provide direct information on performance limiting mechanisms such as mass transport. As shown in Fig. 5(d), the discharge efficiencies for IFF declined quickly with increasing current density, as a result CE of IFF improved and reached up to ~100% at 200 mA/cm^2. This is attributed to its poor mass transport (lowest velocity in the electrode) within the graphite felt matrix, which increases the concentration of either charged or discharged species locally in the felts depending on charge/discharge cycle. Therefore, the single cell reaches the limit for cut-off voltages and charge/discharge cycle ends prematurely. For SFF and CFF, however, CEs reached up to 98% at 200 mA/cm^2 ascribed to the comparatively higher discharge capacity (or longer charge/discharge cycle) due to the improved mass transport.

3.3 Effect of Flow fields on the current – voltage performance of VRFB

A total of 3 different flow fields as mentioned in the earlier section, each coupled with graphite felt electrodes were evaluated. The discharge polarization curves at different flow rates and SOC are presented in Fig. 6 for these flow fields. It should be noted that increasing the flow rate also increases the flow resistance at the inlet and hence the pressure drop. Dennison *et al.* also suggest that the improvement in limiting current density becomes marginal beyond certain flow rates and the limiting current density is an intrinsic property of electrode [24].

Fig. 6 (a, b, c) shows a comparison of the peak power density and current density as a function of voltage and flow rate for different flow fields. It is interesting to note that each flow field displays different polarization behavior even under equivalent experimental conditions. Fig. 6 (a) shows the peak power densities at different flow rates for serpentine flow field. Peak power densities of 0.51, 0.47 and 0.45 Wcm^{-2} were obtained at flow rates of 60, 40 and 20 mL/min, respectively. The IFF (Fig 6 (b)) provides peak power densities of 0.56, 0.55 and 0.53 W/cm^2,

while the CFF (Fig. 6 (c)) provides peak power densities of 0.58, 0.52 and 0.43 W/cm^2 at flow rates of 60, 40 and 20 mL/min, respectively. The current densities at 0.4 V for IFF, SFF and CFFs are 0.76, 0.71, & 0.64, 0.94, 0.82, & 0.68, and 1.24, 1.08, & 0.85 A/cm^2 at 60, 40 and 20 mL/min, respectively. These results are consistent with the calculated electrolyte velocities within the electrodes (Figures 2-4) illustrating its direct relation to the mass transport resistance. Apparently, the IFF shows higher peak power density of 0.53 W/cm^2 at low flow rate of 20 mL/min, which is 15 and 19% higher than that of the SFF and CFF, respectively. However, the current density (at 0.4 V) at 20 mL/min was just 0.64 A/cm^2 which is 6 and 24% lower than that of the SFF and CFF, respectively. It is an indication of the significant mass transport issues associated with IFF even at high flow rates. On the other hand, the mass transport limitation tends to disappear at high flow rates for SFF. Therefore, there is no substantial concentration polarization at 60 mL/min flow rate in case of the cell with SFF. Although, CFF has shown the higher over potential (~100 mV), the obtained current density at 0.4 V for this flow field is 1.24 A/cm^2 which is 24 and 39% higher than that of the SFF and IFF, respectively at 60 mL/min. The over-potential is determined by non-uniform electrolyte distribution in the electrode, therefore, the poorly irrigated area at the corners of CFF represents the higher over potential. As anticipated, increment in the flow rate shifts the mass transport limitation towards higher current density region, which is true for all flow field geometries. The reason behind this shift is the reduced electrolyte residence time with the increase in flow rate [24].

The polarization curves at 100, 75, 50 and 25% SOC for SFF, IFF and CFF are shown as Fig. 6 (d, e and f), respectively. VRFBs are not affected by the deep discharge unlike other primary or secondary batteries, however, flow fields could improve the limiting current density and performance by enhancing the mass transport at lower SOCs. Not all flow fields are equal when

it comes to improve the mass transport. IFF provides attractive power densities at low current densities, on the other hand, it fades rapidly and reaches to mass transport limitation at high current densities. The SFF could obtain a power density of 0.18 W/cm^2 at 0.2 A/cm^2 of current density at 25% SOC, considerably better than CFF. However, this gap quickly disappears and reverses at higher SOCs.

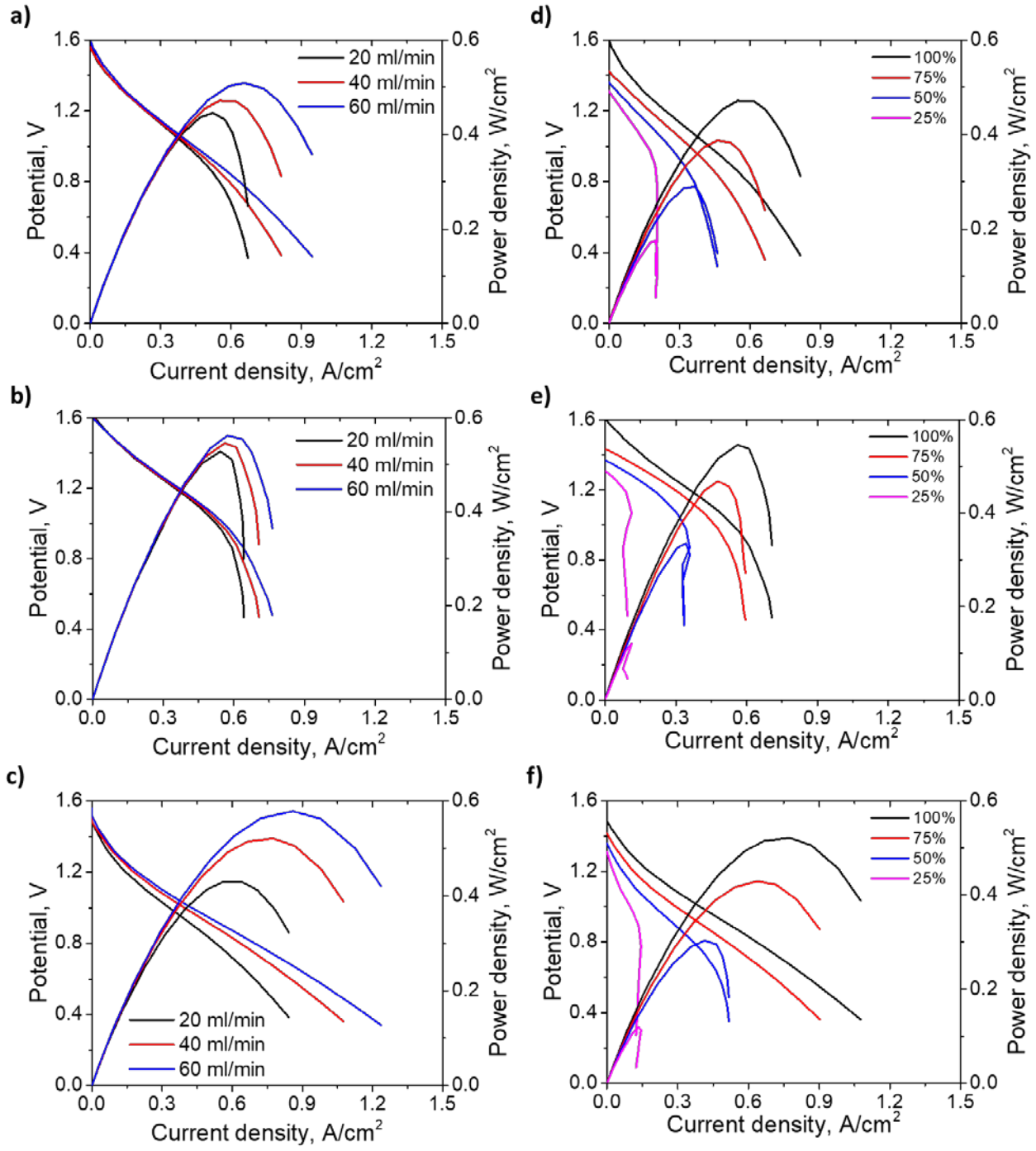

Figure 6. Polarization curves at various flow rates and SOC for cell configured with SFF (a, d), IFF (b, e) and CFF (c, f), respectively.

The electrolyte first flows into the channels and then the electrolyte enters the electrodes in the VRFB cell. Once electrodes are filled with electrolyte, the effect of convective forces present

at the interface of electrode and flow field channels become weak and most of the transport is realized by diffusion. The mass transport limitation is obvious at low flow rate and tends to vanish at high flow rates thanks to the turbulence produced by high electrolyte flow. On the other hand, the mass transport limitation is found to be negligible in CFF even with low flow rate owing to the convective flow through the electrode matrix. These convective forces are responsible for efficient exchange of charged – discharged electrolytes and reduced electrolyte residence time. The flow battery performance in terms of limiting current density and obtained power density reported here is better than the values reported in the literature for thick graphite felt electrodes with or without flow fields [17, 18, 25]. This performance is even comparable to the zero gap carbon paper flow batteries, therefore, we carried out a further comparative study with carbon paper and graphite felt in equivalent conditions.

3.4 Graphite felt vs carbon paper

There have been great disparity between the performances obtained using thick graphite felt electrodes (with or without flow fields) to carbon paper electrodes. The obtained power density is almost three times higher for carbon paper electrode with zero gap design than graphite felt electrode in any design in similar electrolyte condition [26]. Therefore, meticulous analysis of electrochemical performance data obtained from VRFB cell with carbon paper and graphite felt is important for broader perspective.

Fig. 7 compares the electrochemical performance of graphite felt and carbon paper electrodes in VRFB with SFFs. The significance of this cannot be ignored that the graphite felt shows the maximum power density of 0.47 W/cm^2 at 40 mL/min, on the other hand maximum power density obtained for carbon paper was just 0.32 W/cm^2. Comparison of carbon paper and

graphite felt electrode yielded into exciting observation that graphite felt electrodes provide higher power density at low flow rate (flow rate increment was stopped for graphite felt VRFB at 60 mL/min to avoid excessive pressure build up). Increment in flow rate for the carbon paper increases the output power density, however, similar power output is achieved with felt electrodes at low flow rates. It is believed that the thin and dense carbon paper significantly reduces the mass transport limitations and charge transport distances. Hence, it greatly improves the VRFB output. Also, conventional wisdom has it that a thick graphite electrodes have more transport issue, higher over-potential and thus exhibit lower performances. However, in this study we have found that the flow battery output is far inferior with carbon paper than the felt electrodes. The mass transport issues alone cannot explain this distinct trend. Therefore, upon careful dissection of performance and experimental parameters (Table 1), we have proposed the flow velocity, which is ratio of flow rate and effective area as shown below:

$$Flow\ Velocity, cm\ s^{-1} = \frac{Flow\ rate, cm^3\ min^{-1}}{Area, cm^2}$$

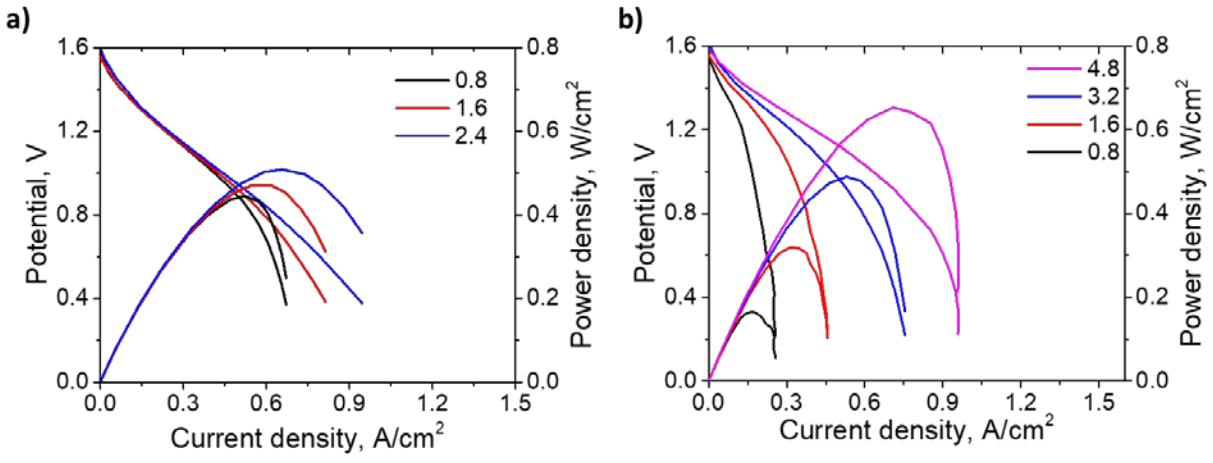

Figure 7. Polarization curves at different flow velocities; (a) SFF-Graphite felt, and (b) SFF-Carbon paper (3- layers of SGL 10 AA used at cathode and anode).

The flow velocity is merely the indicator of electrolyte residence time and concentration polarization for unit area. Higher the flow velocity, the mass transport will be shifted at higher limiting current density owing to the low electrolyte residence time. Flow velocity could certainly explain the lower output power density with felt in previous literature where flow velocity was just 1.14 cm s^{-1}, consequently, the obtained power density were inadequately 0.15 W/cm^2. The obtained power density with respect to flow velocity and other flow battery parameters is presented in table 1. Aaron *et al.* achieved the maximum power density of 0.56 W/cm^2 with the combination of SFF and 3 layers of carbon paper electrode at flow velocity of 4.0 cm s^{-1}. It is also evident that the higher flow velocity results into improved mass transport and hence boosts the power densities. The Fig. 7(b) shows the polarization curves obtained from 0.8 to 4.8 cm s^{-1} of the flow velocity, the power density increased from the 0.18 to 0.46 W/cm^2. These results are in good agreement with the results reported in literature.

Table 1. Summary of performances of VRFBs with different flow fields and carbon electrodes.

Flow Field	**Electrode**	**Flow rate, mL/min**	**Area, cm^2**	**Electrolyte volume, mL**	**Flow Velocity, cm/s**	**Power density, mW/cm^2**	**Reference**
Serpentine	Felt	60	25	120	2.4	510	This work
Interdigitated	Felt	60	25	120	2.4	560	This work
Conventional	Felt	60	25	120	2.4	580	This work
Serpentine	Felt	114	100	160	1.14	150	[18]
Serpentine	Paper	120	25	120	4.8	655	This work
Serpentine	Paper	20	5	100	4.0	557	[26]
Serpentine	Paper	80	5	-	16	460	[24]

The objective of this work to provide insights of mass transport issues due to the flow field geometry. Therefore, we have not compiled data regarding the pressure drop for the flow field geometry. Importantly, the active area of the cell in this study is fairly small (25 cm^2) compare to state of the art VRFBs designed for Megawatt scale (several m^2). Therefore, our group is focusing on the scaling up the system numerically to study the concentration polarization and pressure drop for different flow fields. It should reflect in our subsequent publications.

Conclusions:

In this work, we have investigated the effects of flow fields on the performance of VRFBs. Besides, the effect of flow rate and SOC on the obtained power density is also studied. The results indicate that the most hailed IFFs hold significant mass transport losses at higher current densities. Although the CFF displayed best power density, the maximum depth of discharge it can achieve is lower than that of the SFF. The electrolyte flow through thick electrode significantly reduces the electrolyte residence time; as a result, it improves the mass transport limitation that reflects the improved power density and limiting current density. It is well supported by our simulation study where we found that the flow velocity is highest in the CFF and hence electrolyte distribution. Each flow field has an optimized flow rate and operating conditions at which maximum performance can be achieved. At low current density and flow rates, interdigitated flow filed demonstrated significantly higher performance, however, the performance gap between interdigitated and other flow fields was eased and overturned with increase in flow rate or current density. Here, we have proposed the flow velocity, derived from the individual cell area and flow rate, to explain the discrepancy in the carbon paper and graphite

electrode performance in the equivalent systems. It is expected that the insights gained in this study may provide engineers and researcher information on optimization of high power density flow batteries.

Acknowledgement

This work is supported by Laboratory Directed Research & Development, Los Alamos National Laboratory (LANL).

Reference

[1] D.C. Holzman, Environmental Health Perspectives, 115 (2007) A358-A361.
[2] C. Ding, H. Zhang, X. Li, T. Liu, F. Xing, J. Phys. Chem. Lett., 4 (2013) 1281-1294.
[3] S. Maurya, S.-H. Shin, Y. Kim, S.-H. Moon, RSC Advances, 5 (2015) 37206-37230.
[4] A. Parasuraman, T.M. Lim, C. Menictas, M. Skyllas-Kazacos, Electrochimica Acta, 101 (2013) 27-40.
[5] M.L. Perry, A.Z. Weber, Journal of the Electrochemical Society, 163 (2016) A5064-A5067.
[6] T. Shigematsu, T. Kumamoto, H. Deguchi, T. Hara, 2 (2002) 1065-1070.
[7] M. Ulaganathan, V. Aravindan, Q. Yan, S. Madhavi, M. Skyllas-Kazacos, T.M. Lim, Advanced Materials Interfaces, 3 (2016).
[8] Z. Yang, J. Zhang, M.C.W. Kintner-Meyer, X. Lu, D. Choi, J.P. Lemmon, J. Liu, Chemical Reviews, 111 (2011) 3577-3613.
[9] S. Maurya, S.H. Shin, J.Y. Lee, Y. Kim, S.H. Moon, RSC Advances, 6 (2016) 5198-5204.
[10] A.M. Pezeshki, Z.J. Tang, C. Fujimoto, C.-N. Sun, M.M. Mench, T.A. Zawodzinski, Journal of the Electrochemical Society, 163 (2016) A5154-A5162.
[11] X.L. Zhou, T.S. Zhao, L. An, L. Wei, C. Zhang, Electrochimica Acta, 153 (2015) 492-498.
[12] H. Zhang, C. Ding, J. Cao, W. Xu, X. Li, H. Zhang, Journal of Materials Chemistry A, 2 (2014) 9524-9531.
[13] S.-J. Seo, B.-C. Kim, K.-W. Sung, J. Shim, J.-D. Jeon, K.-H. Shin, S.-H. Shin, S.-H. Yun, J.-Y. Lee, S.-H. Moon, Journal of Membrane Science, 428 (2013) 17-23.
[14] L. Li, S. Kim, W. Wang, M. Vijayakumar, Z. Nie, B. Chen, J. Zhang, G. Xia, J. Hu, G. Graff, J. Liu, Z. Yang, Advanced Energy Materials, 1 (2011) 394-400.
[15] B. Dunn, H. Kamath, J.-M. Tarascon, Science, 334 (2011) 928.
[16] Q.H. Liu, G.M. Grim, A.B. Papandrew, A. Turhan, T.A. Zawodzinski, M.M. Mench, Journal of The Electrochemical Society, 159 (2012) A1246-A1252.
[17] Q. Xu, T.S. Zhao, C. Zhang, Electrochimica Acta, 142 (2014) 61-67.
[18] S. Kumar, S. Jayanti, Journal of Power Sources, 307 (2016) 782-787.
[19] X. Ke, J.I.D. Alexander, J.M. Prahl, R.F. Savinell, Journal of Power Sources, 270 (2014) 646-657.
[20] J.T. Davies, J.J. Tummino, C, 4 (2018).
[21] E. Knudsen, P. Albertus, K.T. Cho, A.Z. Weber, A. Kojic, Journal of Power Sources, 299 (2015) 617-628.
[22] P.T. Nguyen, T. Berning, N. Djilali, Journal of Power Sources, 130 (2004) 149-157.
[23] R.M. Darling, M.L. Perry, Journal of the Electrochemical Society, 161 (2014) A1381-A1387.

[24] C.R. Dennison, E. Agar, B. Akuzum, E.C. Kumbur, Journal of the Electrochemical Society, 163 (2016) A5163-A5169.
[25] J.Q. Chen, B.G. Wang, H.L. Lv, in, 2011, pp. 604-607.
[26] D.S. Aaron, Q. Liu, Z. Tang, G.M. Grim, A.B. Papandrew, A. Turhan, T.A. Zawodzinski, M.M. Mench, Journal of Power Sources, 206 (2012) 450-453.